CHAPTER IV
STEAM REFORMING OF METHANOL OVER GDC AND METAL LOADED GDC CATALYSTS PREPARED VIA SOL-GEL ROUTE

4.1 Abastract

GDC and metal (viz. nickel and copper) loaded GDC were synthesized using the sol-gel method. The amount of gadolinium doped to ceria was fixed at 10 % mole. Cu and Ni were chosen metal catalyst. The influence of hydrolysis molar ratio (*h*) and acid molar ratio (*A*) were found to affect the gel formation. The *h* and *A* condition, 29 and 0.3, respectively, were selected to synthesize all catalysts. Various analyzing techniques, including TGA, XRD, BET, SEM, EDX, and TPR, were employed to characterize the obtained products. All products calcined at 500 °C were found to have fine crystallite size and high homogeneity. Their catalytic activities on methanol steam reforming were carried out in the temperature range 200–400 °C. The activity of GDC10 was compared with those of 10 % Ni/GDC10, 20 % Ni/GDC10, 10 % Cu/GDC10, and 20 % Cu/GDC10. 20 %Ni/GDC10 showed the highest activity at 400 °C, over 70 % methanol conversion.

Keywords : GDC, Steam reforming, Sol-gel process, Methanol

4.2 Introduction

Due to economical and environmental issues of traditional fossil energy, nowadays, the development of alternative renewable energy has been focused. Hydrogen energy is an important fuel in the future for use as an energy carrier for electric vehicles and electric plants. There are several processes to produce hydrogen, and one of promising processes is methanol steam reforming. The majority of the catalytic steam reforming of methanol has been focused on Cu-based catalysts. Although most interesting catalysts for the methanol steam reforming are on $CuO/ZnO/Al_2O_3$ based catalysts [1], Liu *et al.* reported that Cu/CeO_2 catalyst showed

higher activity than Cu/ZnO, Cu/Zn(Al)O, and Cu/Al_2O_3 catalysts with the same Cu loading under the same reaction conditions [2]. However, copper is still found to have some significant drawbacks, such as fast deactivation. Thus, other based catalysts of group VIII metals, such as Pd, Pt, and Ni, have been investigated to overcome such the drawback [3]. Kikuchi *et al.* studied the catalytic activity of Ni on the methanol steam reforming and suggested that Ni/Al_2O_3 catalyst showed stable activity at 723 K, but relatively low hydrogen yield because of methanation among other catalysts [4]. Thermal stablility and carbon deposition resistivity of Ni/CeO_2 were better than Ni/Al_2O_3, as suggested by Dokmaingam *et al.* [5].

Doping Gd to ceria has also been considerable interest since the ionic radii of Gd^{3+} is nearly the same as Ce^{4+}. Doping Gd to ceria lattice can create more oxygen ion vacancies, leading to higher ionic conductivity than un-doped ceria [6]. In this work, the methanol steam reforming on gadolinium-doped ceria (GDC) and metal loaded GDC catalysts was investigated. Sol-gel technique was selected to synthesize the catalysts while Cu and Ni were chosen to be loading metals.

4.3 Experimental

4.3.1 Catalyst Preparation

Cerium glycolate complex was synthesized via oxide one-pot synthesis (OOPS) process [7]. The preparation was modified by tripling the scale reported by Ksapabutr *et al.* (2004), i.e. mixing 3.12 g of cerium (IV) hydroxide ($Ce(OH)_4$, Aldrich), 54 mL of ethylene glycol (EG, J.T. Baker), and 2.19 g of triethylenetetramine (TETA, Facai Polytech) with sodium hydroxide (NaOH, Merck) at about 12 mole% equivalents to cerium hydroxide. The mixture was magnetically stirred and heated to the boiling point of EG for 18 h under nitrogen to distill off EG and water liberated from the reaction. The reaction mixture was cooled overnight under nitrogen. The precipitated product was filtered and washed with acetonitrile (Lab-Scan), followed by drying under vacuum.

In this study the amount of gadolinium doped to ceria was fixed at 10% mole. The metal complex sources used were cupric acetate monohydrate

($Cu(CH_3COO_2).H_2O$, 99 % — Fluka), gadolinium (III) nitrate hexahydrate ($Gd(NO_3).6H_2O$, 99.9 % — Aldrich), and nickel (II) acetate tetrahydrate ($Ni(CH_3COO)_2.4H_2O$, 98 %—Aldrich). Gadolidium-doped ceria, nikel loaded gadolidium-doped ceria and cupper loaded gadolidium-doped ceria were prepared via sol-gel method by hydrolyzing cerium glycolate precursor in the mixture of metal complex, nitric acid (HNO_3, 65 % Lab-Scan), and water. In this work, the effects of solvent and acid amounts on gel formation was investigated. The amounts of starting materials depended on the hydrolysis molar ratio (h = H_2O/Ce) and acid molar ratio (A = acid/Ce) while loaded metals were studied at 10 and 20 mole percent. The gelation reaction was carried out at room temperature with continuously stirring at the suitable mole ratio of acid and solvent. Soft gel was obtained after aging for 1 h at room temperature. All produced powders were obtained by thermal treatment in a furnace at 500 °C for 7 h. The samples were ground and sieved to 80–120 mesh size. Figure 4.1 presents a flow diagram of the synthetic route.

4.3.2 Characterization

Cerium glycolate precursor was characterized by a TG/DTA (Perkin-Elmer Pyris Diamond) with a heating rate of 10 °C/min from 30 °C to 800 °C and a FTIR (Nicolet, Nexus 670) at the wave number range of 4000–400 cm^{-1} and the resolution of 4 cm^{-1} with 32 scans. The TG/DTA was also used to determine organic residue of the calcined powders. The crystalline structure and phase composition of samples were characterized using x-ray diffraction (XRD, Rigaku, Rint 2200HV) with Cu-Kα radiation operated at 40 kV and 30 mA on the 2θ range from 20-100° at a scanning speed of 5°/min with a scan step of 0.02°. Surface area of the calcined powder was analyzed on Thermo Finnigan, Sorptomatic 1990 using Brunauer-Emmett-Teller (BET) method. The samples were outgassed to remove moisture adsorbed on the surface at 250 °C before analysis. Morphology of the synthesized products was examined by scanning electron microscope (SEM, Hitachi, S–4800). Energy dispersive X-ray spectroscopy (EDX) was used to observe element dispersion on the samples. Temperature programmed reduction (TPR) experiments were performed under a flow of a 5 % H_2 in Ar mixture (30 ml/min) over 0.05 g of catalyst using a heating rate of 10 °C/min. Before the reduction, the system was

purged while being heated to 150 °C with 4 °C/min for 1 h and cooled to 30 °C by flowing 10 ml/min of nitrogen for eliminating moisture. The thermal conductivity detector (SRI model 110) was used to monitor hydrogen contents before and after the reduction. The amount of carbon deposited on spent catalyst was measured by temperature programmed oxidation (TPO) performed under a flow of a 2 % O_2 in He mixture (30 ml/min) over 0.03 g of catalyst using a heating rate of 10 °C/min. Carbon formation was oxidized into carbon dioxide which was converted to methane in a methanator. The product gas was analyzed by a gas chromatograph (Shimadzu, GC-17A) equipped with a flame ionized detector (FID).

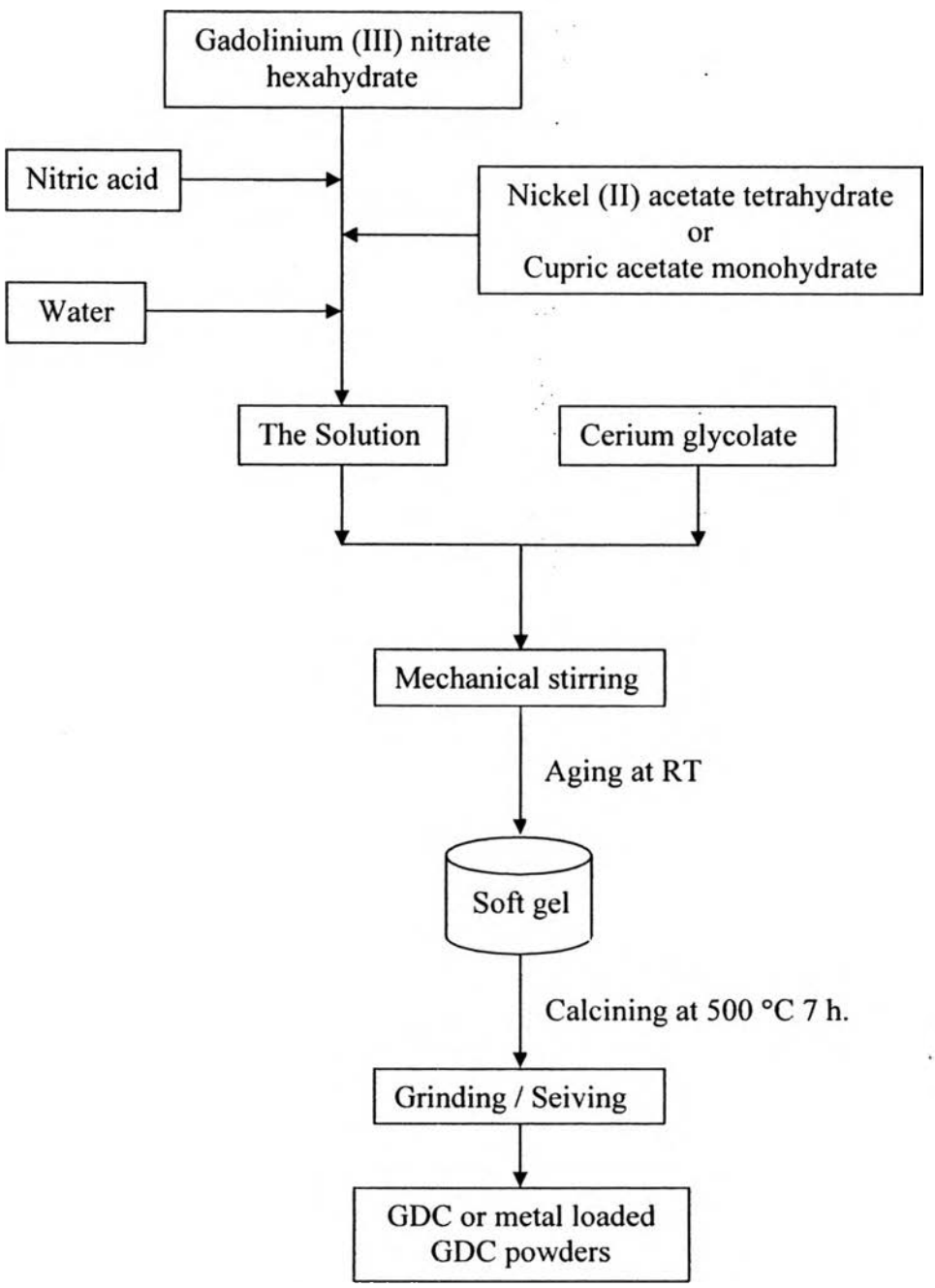

Figure 4.1 Flowchart illustrating the synthetic route to GDC and metal loaded GDC powders via the sol-gel technique.

4.3.3 Catalytic Activity

The catalytic test was conducted using a fixed-bed flow reactor at at atmospheric pressure and in the temperature range of 200–400°C. A 0.1 g sample of the catalyst (80–120 mesh size) was packed in a vertical pyrex glass microreactor with an inside diameter of 8 mm. The reactor was installed and electronically heated in the furnace. The temperature of the catalyst bed was controlled and monitored by PID temperature controller equipped with a chromel-alumel thermocouple (Type K). The mixture of water and methanol (CH_3OH, 99.8 %—Lab-Scan) was injected by syringe pump at a rate of 1.5 mL/h to a vaporizer. The methanol vapor and steam were carried by helium with a flow rate of He. being kept at a constant gas space velocity (GHSV) of 14008 mL/g-cat h. Steam to methanol ratio ($MeOH:H_2O$) was set at 1.5 [8]. The product gases were analyzed by a Hewlett Packard 5890 series II gas chromatograph equipped with a thermal conductivity detector (TCD). The column utilized in a gas chromatograph was Carbosphere®, 80/100 mesh, 10 ft x 1/8 inch stainless steel packed column. The results were recorded by Agilent Chemstation software. The observed peaks were identified by comparison with the retention time of the standard gas. For quantitative analysis, the peak area was used to determine the concentration of each component, based on the calibration curves obtained from known composition gases.

4.4 Results and discussion

4.4.1 Systhesis of Cerium Glycolate

To obtain high percentage yield of cerium glycolate, EG was served excessively. It was used not only as a solvent, but also as a reactant to form bidentate chelates for cerium. Moreover, an excess of EG also acted as a carrier to remove water from the system and to drive the reaction forward. TETA and NaOH were

employed as catalyst and co-catalyst, respectively. FTIR spectrum of cerium glycolate is given in Figure 4.2. The peak at 1080 cm^{-1} was referred to the Ce–O–C stretching vibration, and the band at 570 cm^{-1} was corresponding to the Ce–O stretching [7, 9]. The OH bands at 3700–3000 and 1600 cm^{-1} were ascribed as the O–H stretching and bending vibrations of water absorbed from the moisture in the air.

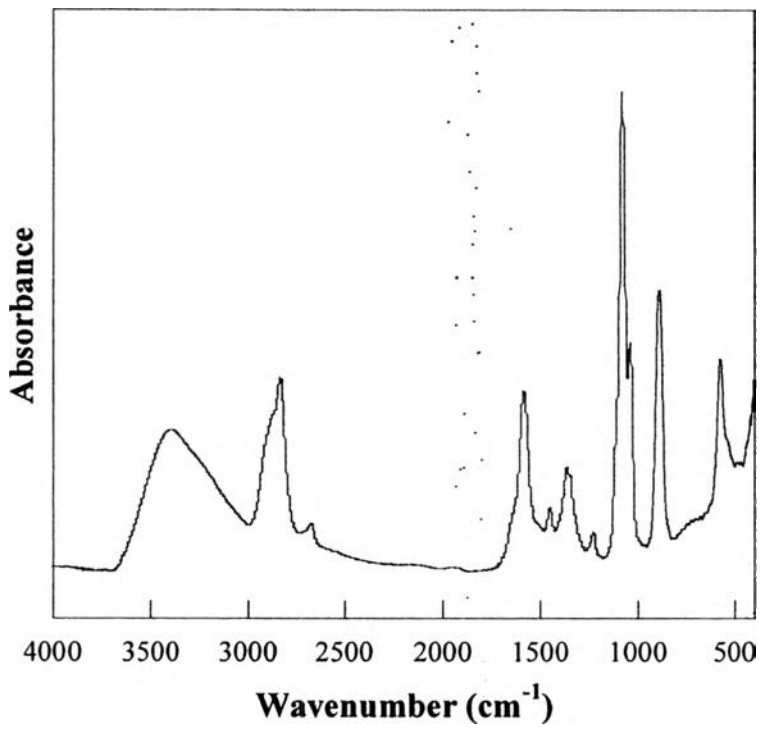

Figure 4.2 FTIR spectrum of cerium glycolate.

Thermograms of the product are shown in Figure 4.3. It obviously exhibits transition region around 350–500 °C owing to the glycolate decomposition. The product's weight loss and ceramic yield were 33.9 % and 66.9 % which are in agreement with the work of Ksapabutr *et al.* [7].

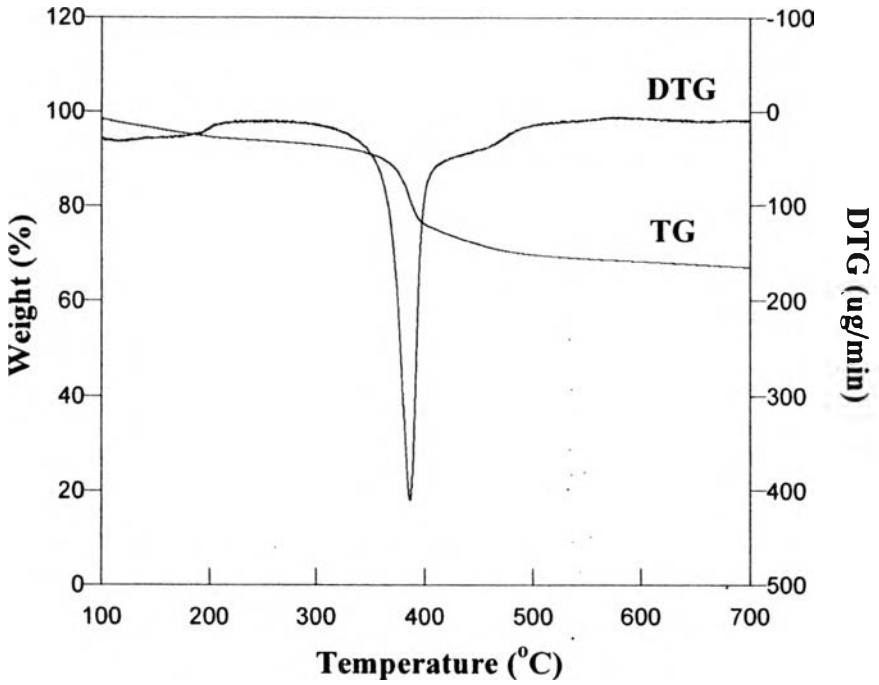

Figure 4.3 TG–DTG thermograms of cerium glycolate complex.

4.4.2 Synthesis of Gadolidium–doped Ceria and Metal Loaded Gadolidium–doped Ceria

4.4.2.1 Effect of Solvent and Acid Amounts on Gel formation

In this study, ($Gd(NO_3).6H_2O$ and metal acetate were dissolved in HNO_3, followed by adding water as solvent before adding cerium glycolate. Metal acetate and cerium glycolate were protonated by nitric acid, enhancing the reaction kinetics by producing good leaving group [10]. Both hydrolysis and condensation reactions occurred to produce metal-oxygen-metal network, as following;

Hydrolysis:

$$M(OR)_n + xH_2O \rightarrow M(OH)_x(OR)_{n-1} + xROH \quad (1)$$

Condensation:

$$—M—OH + HO—M— \rightarrow —M—O—M— + H_2O \quad (2a)$$

—M—OH + RO—M— → —M—O—M— + ROH (2b)

The hydrolysis and condensation of cerium glycolate was controlled by hydrolysis molar ratio (h = H_2O/Ce), acid molar ratio (A = acid/Ce), gelation time, and chemical composition [11, 12]. Gel formation was studied by varying the hydrolysis molar ratio and acid molar ratio in the range of 20–70 and 0–0.5, respectively. For 10 % Ni/GDC10, when h and A were increased from 25–70 and 0.3–0.4 ratios, respectively, a cloudy yellow solution first occurred, followed by the formation of dark brown gel in 60 min, as shown in Figure 4.4. For 10 % Cu/GDC10, when h = 25–70 and A = 0.3–0.4, green gel was resulted in 120 min. However, when amount of loading metal increased from 10 to 20 % the gelation time of 20 % Cu/GDC10 took longer (180 min) while the gelation time of 20 % Ni/GDC10 was increased to 240 min. This phenomenon was due to acidity of copper ion is higher than that of nickel ion. Once increase of the amount of copper, the acidity became higher. Thus, the hydrolysis reaction was enhanced and shifted to the right to form hydroxo ligands, M-OH, driving the condensation process [11, 13]. From Figure 4.4, it can be concluded that at low acid molar ratio the hydrolysis was slow and became faster with increasing amount of acid molar ratios due to more protonated –OR ligand of metal, providing a better leaving group. However, increasing the amount of water, the condensation rate became slower due to the reversed hydrolysis and the decrease in the acid concentration [11]. Moreover, the addition of more nitric acid did not only speed up the hydrolysis rate, but decrease the rate of condensation. Since more acid is added to the system, more hydroxo ligands are protonated to form $M\text{-}OH_2^+$, causing loss of nucleophilicity of the oxygen atom [10, 11].

From the work of Chalermnontakarn *et al.* [14], calcined powder using various acids and solvents gave no obvious difference in BET surface area and particle size. Therefore, in this work, one gel condition for catalytic study was selected to synthesize all catalysts, using h = 29 and A = 0.3, in which the obtained GDC10 provided a cloudy yellowish soft gel.

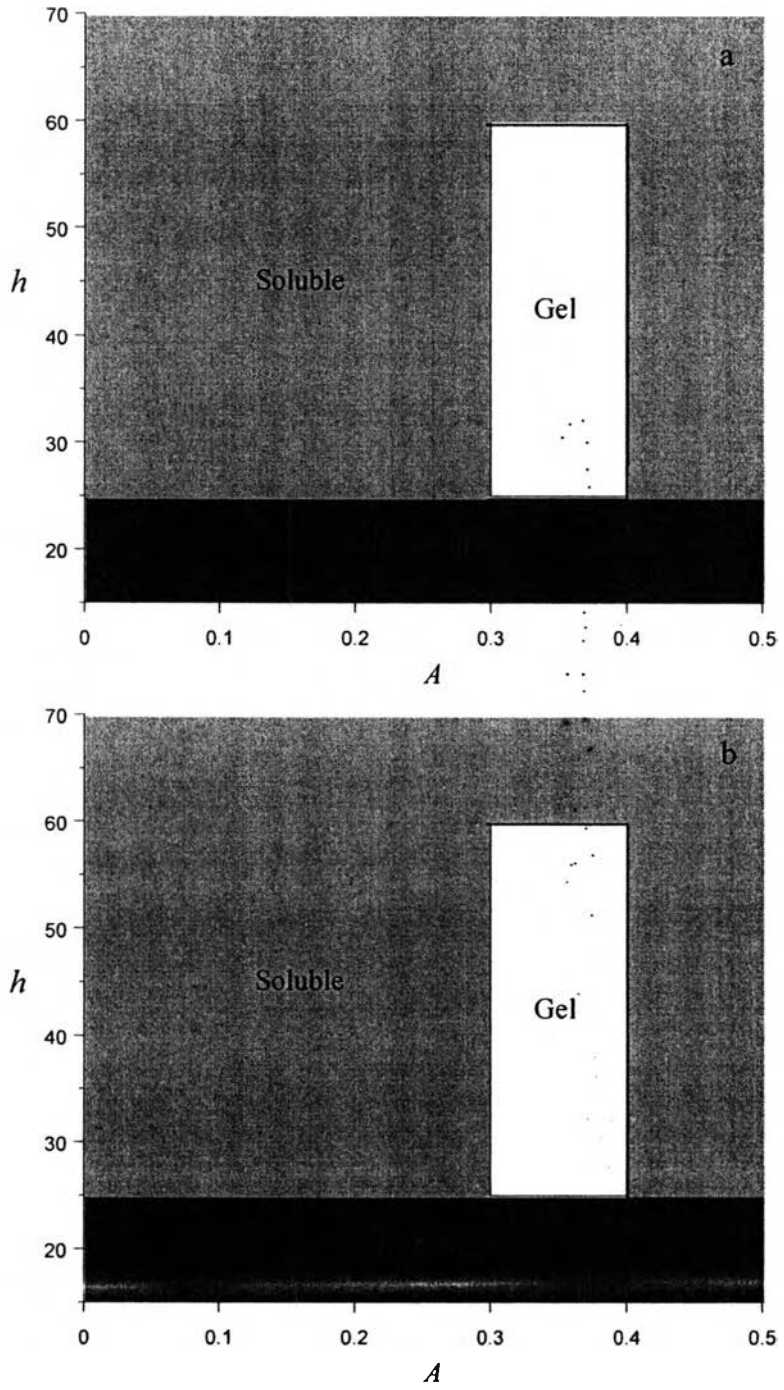

Figure 4.4 Effect of hydrolysis molar ratio (h) and acid molar ratio (A) on gel formation of: (a) 10 % Ni/GDC10 and (b) 10 % Cu/GDC10.

4.4.3 Powder Characterization

Figure 4.5 shows the TGA thermogram of calcined samples, showing no weight loss at any temperature in the range of 30 °C to 700 °C with 100% ceramic yield. It implies that there is no organic residue after calcination at 500 °C for 7 h.

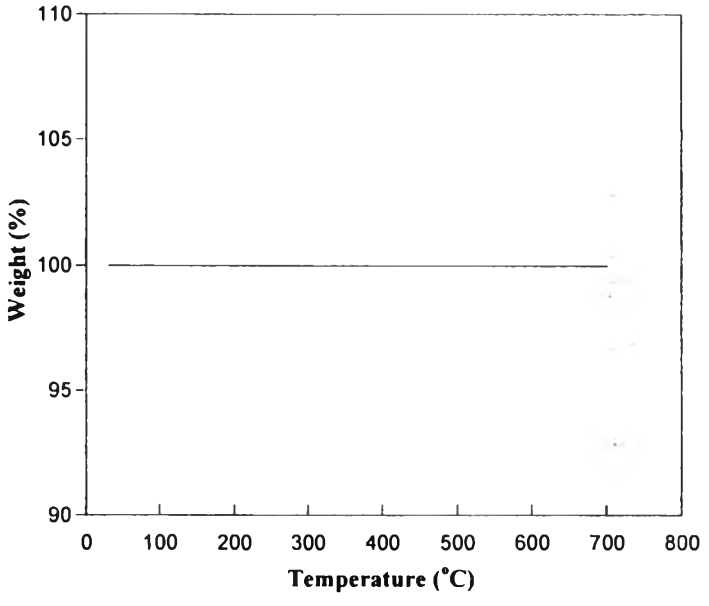

Figure 4.5 The TGA thermogram of 20 % Ni/GDC10 at 500 °C for 7 h.

The XRD patterns of calcined samples are shown in Figure 4.6. All samples show the same pattern, exhibiting main reflections of cubic fluorite structure of GDC, corresponding to {111}, {200}, {220}, and {311} planes which are in good agreement with JCPDS No. 75-0161 [14, 15]. It can be seen that no crystalline phases, corresponding to Gd_2O_3, NiO, and CuO, occur, indicating homogeneity of the mixed oxides and good distribution[16-18]. The crystallite size of all samples was estimated using the Scherrer equation. Those peaks are quite broad, indicating that the crystallite size was very small [19]. They had no significant difference of the size, as listed in Table 4.1. The addition of Ni and Cu provoked a decrease in the specific surface area, and the larger amounts of the loading metal, the more decrease of the surface area [8].

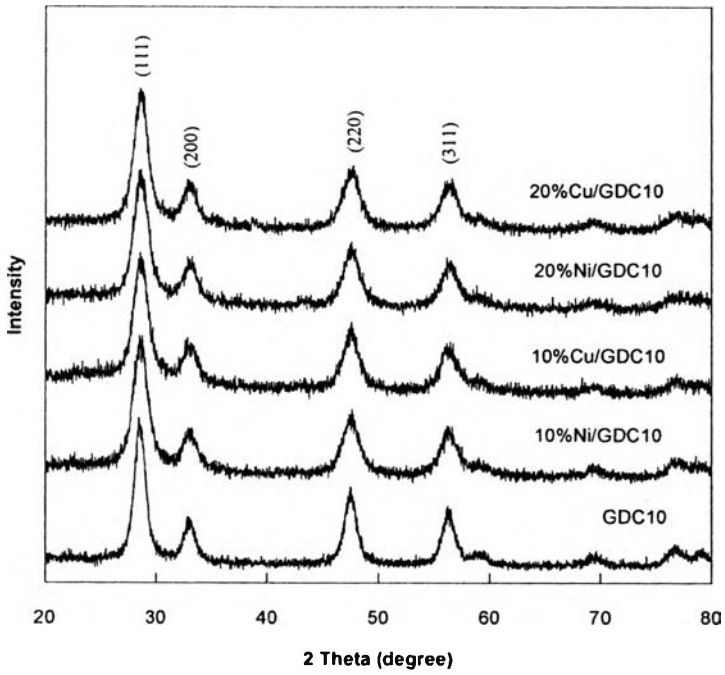

Figure 4.6 XRD patterns of calcined powders: GDC10, 10%Ni/GDC10, 10%Cu/GDC10, 20%Ni/GDC10 and 20% Cu/GDC10.

Table 4.1 BET surface area and crystallite size of all catalysts

Sample	BET surface area (m^2/g)	Crystallite size (nm)				
		111	200	220	311	Average
GDC10	41.51	7.58	7.21	7.71	9.30	7.95
10%Ni/GDC10	20.97	5.13	5.57	7.40	9.09	6.87
20%Ni/GDC10	12.60	6.27	8.00	5.93	8.89	7.27
10%Cu/GDC10	10.79	6.17	6.81	7.41	12.11	8.12
20%Cu/GDC10	5.89	6.27	5.75	7.71	13.32	8.26

Examples of the powder morphology are shown in Figure 4.7. It is observed that the samples have small particle size less than 1 μm, supporting the XRD results. Moreover, metal loaded GDC10 showed denser morphology than

GDC10, corresponding to BET surface area. Distribution of each element presented in Figure 4.8 was found to be highly homogeneous and well-dispersed.

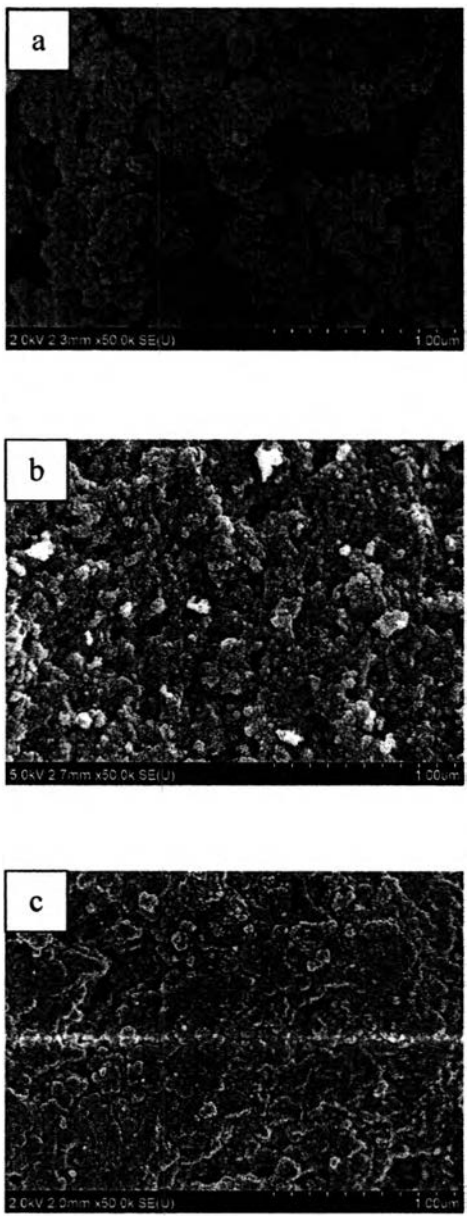

Figure 4.7 SEM images of the powders calcined at 500 °C for 7 h. (a) GDC10, (b) 20%Ni/GDC10 and (c) 20%Cu/GDC10.

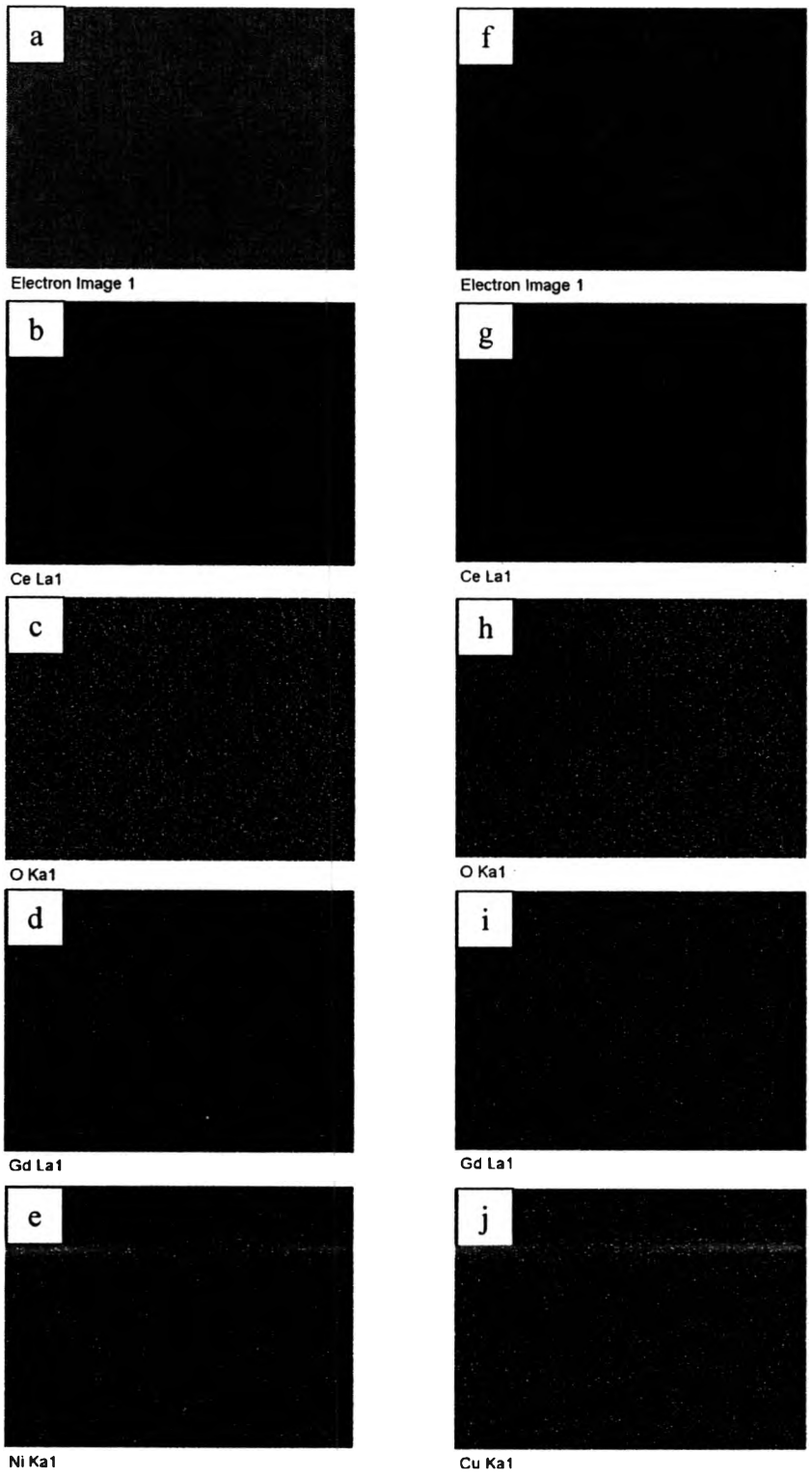

Figure 4.8 SEM images with EDX mappings of: (a-e) 20%Ni/GDC10, (f-j) 20%Cu/GDC.

The H_2-TPR profiles of the samples are shown in Figure 4.9. For GDC10 without any metal loading, it exhibited two reduction peaks appearing at around 530 °C and 800 °C. The first peak is the reduction of the surface capping oxygen of GDC10 whereas the other one is considered to be the reduction of its bulk lattice oxygen [20, 21]. With the presence of metal loaded in GDC10, the first peak at 530 °C disappears. This phenomenon is proposed to be the surface capping oxygen shared with the loaded metal [20]. That is the reason why the occurrence peak at 530 °C of plain GDC10 disappears with the loaded GDC10.

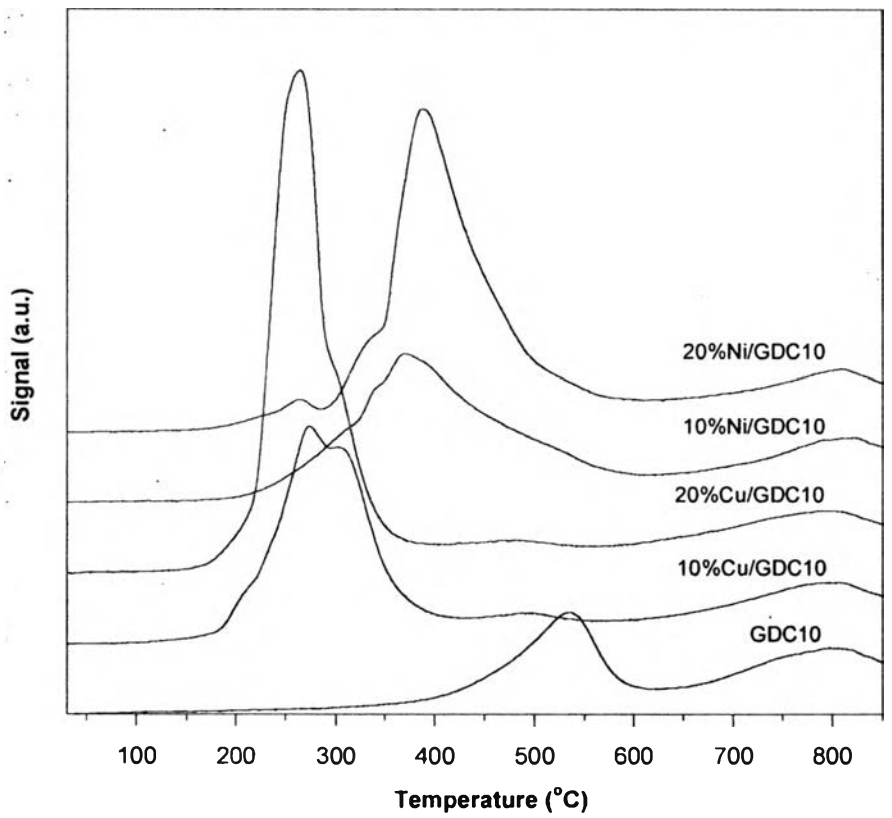

Figure 4.9 TPR profiles of GDC10, copper, and nickel loaded GDC10.

For copper loaded GDC10, there are two overlapping reduction regions at ~300 °C and ~260 °C (high-intensity peak) with a shoulder peak at ~200 °C. According to the work of Avgouropoulos *et al.* [22], the two peaks (~200 °C and ~260 °C) probably represented the reduction of CuO species associated with ceria. Another peak (~300 °C) may be attributed to the reduction of bulk CuO species.

From the previous report by Pengpanich [23], NiO species over CeO_2 could be reduced at ~360 °C. However, in our case, the TPR profile of the nickel loaded GDC10 showed a strong peak at ~380 °C. The 20 °C shift of the reduced NiO temperature was due to a higher interaction between NiO and support [23-24]. Moreover, increasing nickel content to 20%, a small peak at ~250 °C was observed probably due to the hydrogen spillover effect [23].

4.4.4 Catalytic Activity

From Figure 4.10, GDC10 showed no activity on methanol steam reforming whereas the activities of the others increased with the reaction temperature, corresponding to endothermic reaction of the steam reforming [25]. It can be seen that loaded metal was the main active species, moreover, increasing the loadings led to an increase in the activities [26, 27]. The maximum methanol conversion was attained with 20 % Ni/GDC10 at 400 °C. The highest methanol conversion and hydrogen yield exceeded 70 % and 50 %, respectively. However, at lower temperature (300–350 °C), 20 % Cu/GDC10 exhibited a better performance. Many researchers [1, 8, 28] reported that copper based catalyst for the methanol steam reforming showed a good performance at moderate temperature (300–350 °C). High temperature causes deactivation of copper catalysts due to thermal sintering [29]. On the other hand, nickel based catalysts performed catalytic activity at high temperature [30, 31], thus, an increase in operating temperature resulted in higher activity [32]. Furthermore, the TPR results demonstrated the reduction temperature, confirming the catalytic activity results. The study of the nickel based catalyst on the methanol steam reforming reported by Qi *et al.* [33] indicated the potential in the temperature range of ~300–400 °C, corresponding to our results.

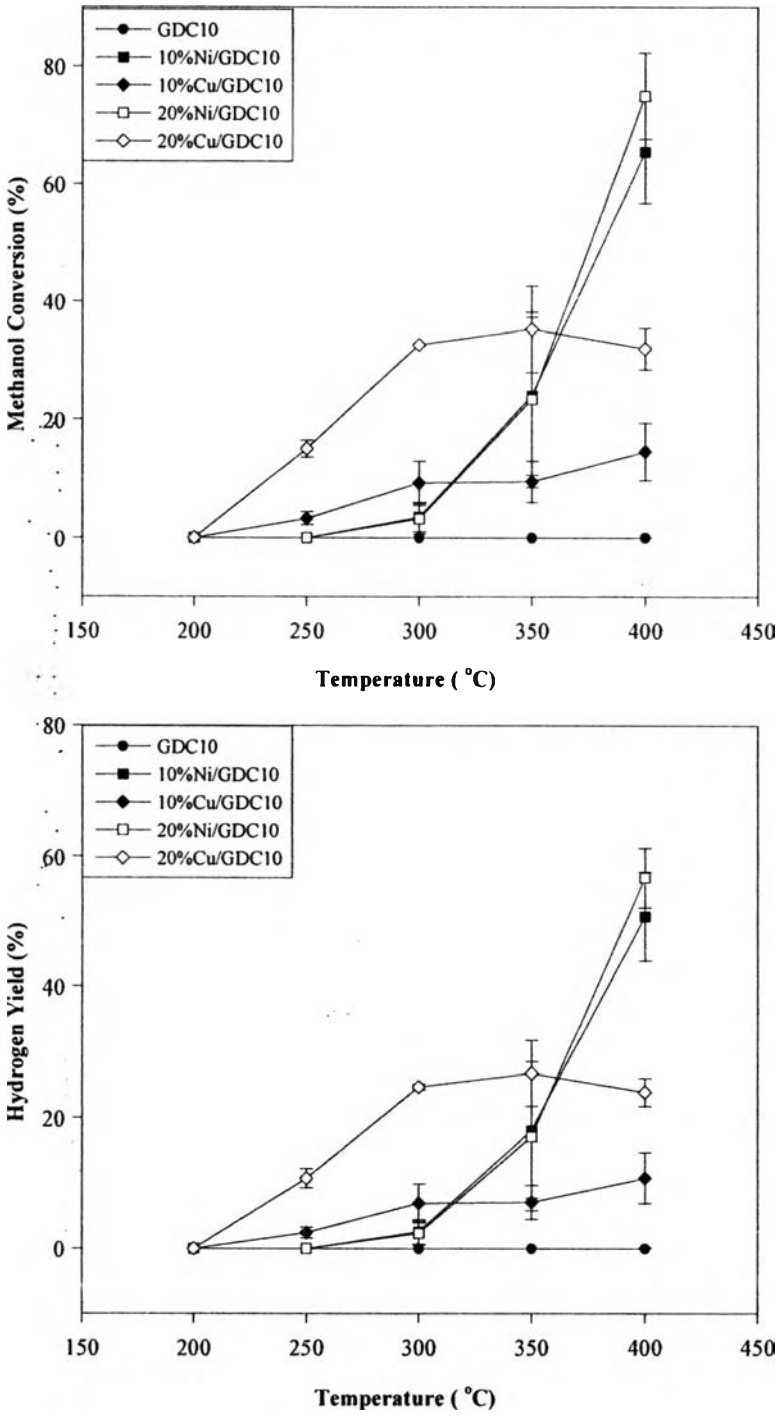

Figure 4.10 Effect of temperature on the methanol conversion and the hydrogen yield over catalysts calcined at 500 °C for 7h.

The selectivity of copper and nickel loaded catalysts are shown in Figures 4.11 and 4.12, respectively.

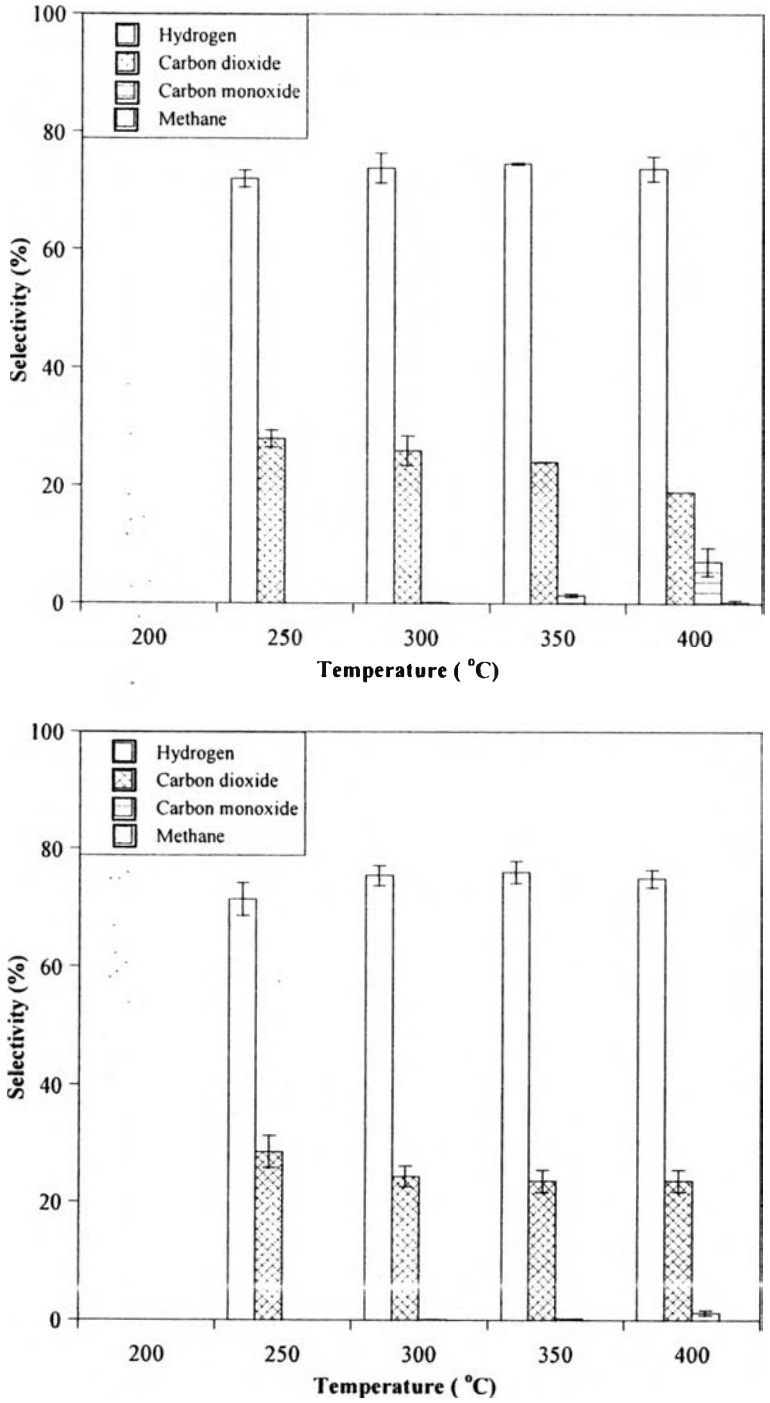

Figure 4.11 Selectivity of copper loaded catalysts: (a) 10 % Cu/GDC10 and (b) 20 % Cu/GDC10.

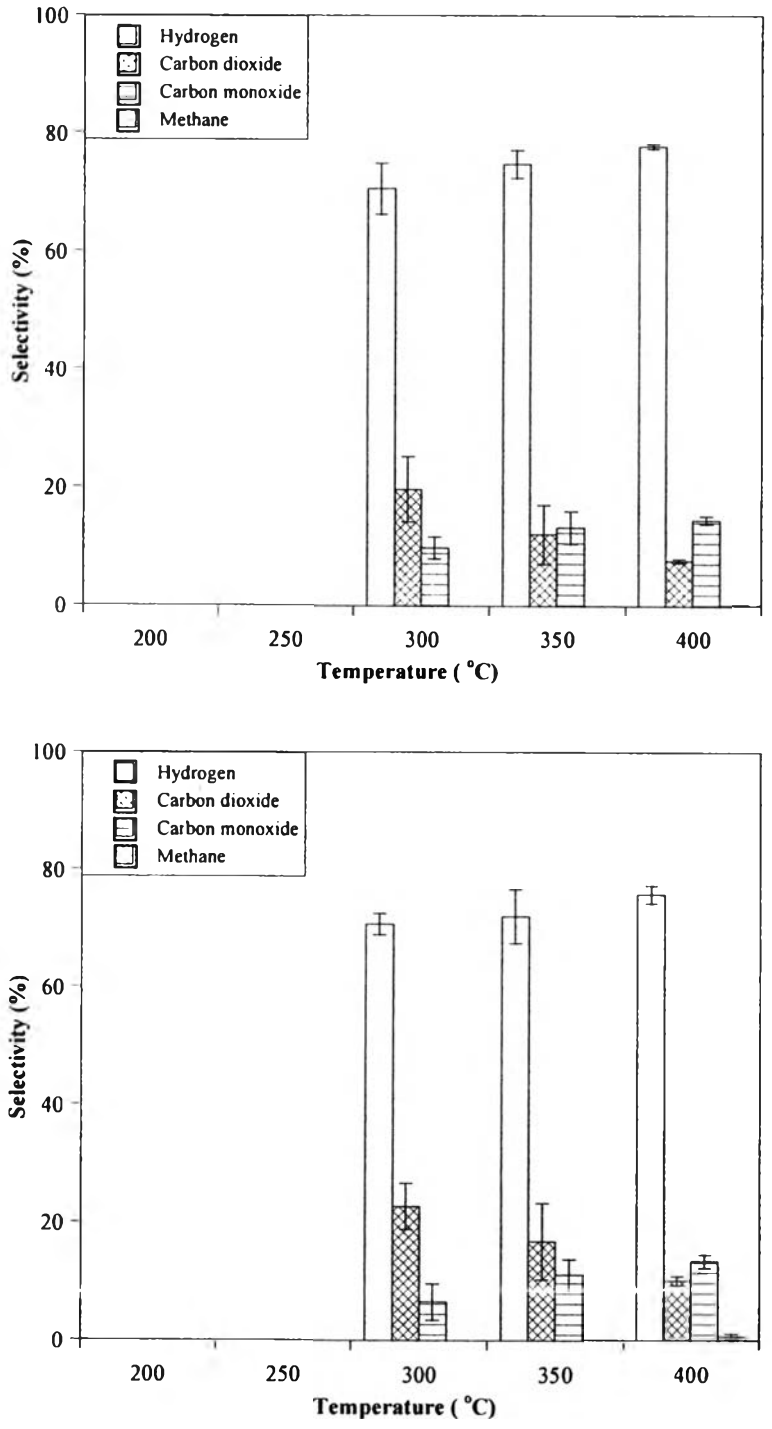

Figure 4.12 Selectivity of nickel loaded catalysts: (a) 10 % Ni/GDC10 and (b) 20 % Ni/GDC10.

It can be seen that hydrogen selectivity of all catalysts were exceed 70% and carbon monoxide was the main by product. Furthermore, carbon monoxide

selectivity increased with temperature whereas carbon dioxide selectivity decreased. This is due to acceleration of reverse water gas shift reaction expressed in Eq.3 [34. 35]. Comparing carbon monoxide selectivity between two metals, nickel loaded catalysts had the higher selectivity, predominately catalyzing methanol decomposition reaction, as expressed in Eq.4 [3, 36].

$$CO_2(g) + H_2(g) \rightarrow CO(g) + H_2O\,(g) \qquad \Delta H°_R = 41\ kJmol^{-1} \qquad (3)$$

$$CH_3OH(g) \rightarrow 2H_2(g) + CO(g) \qquad (4)$$

It was noted that small amount of methane (<1%) was also observed on these catalysts at 400 °C, except 20 % Cu/GDC10. This result might be due to methanation reaction expressed in Eq.5 [4].

$$CO(g) + 3H_2(g) \rightarrow CH_4(g) + H_2O\,(g) \qquad (5)$$

Coke formation on spent catalysts are shown in Table 4.2. It can be seen that all catalysts had small amount of coke, especially, copper-based catalysts showed relatively low coke formation, and an increase of the copper content led to a decrease in coke deposition. However, as increasing nickel content, higher coke deposition was found. This result agrees with the study of Chalermnontakarn *et al.* [14]. The carbon may be formed by the Boudart reaction (Eq.6), as follow [2, 29]:

$$2CO(g) \rightarrow C(s) + CO_2\,(g) \qquad (6)$$

Table 4.2 Amount of coke deposition on the catalysts

Sample	Coke deposition (%)
GDC10	0.42
10%Ni/GDC10	0.30
20%Ni/GDC10	1.56
10%Cu/GDC10	0.19
20%Cu/GDC10	0.12

4.5 Conclusions

GDC10 and metal (Ni and Cu) loaded GDC10 were successfully prepared by sol-gel process, using cerium glycolate as precursor. The suitable condition for the gel formation was hydrolysis molar ratio (h) and acid molar ratio (A) in the range of 20-70 and 0-0.5, respectively. The acidity of metal affected to the gelation time. This synthesis route provided homogeneous particles in the nano-scale. The activity of GDC10 on the methanol steam reforming was very low, as compared to copper loaded GDC10, demonstrating good activity at moderate temperature (250–350 °C) while nickel loaded GDC10 showed good performance at higher temperature (400 °C). All metal loaded catalysts showed the hydrogen selectivity over 70%. The highest methanol conversion and hydrogen yield were achieved by 20%Ni/GDC10. All spent catalysts had small amount of coke deposition in which 20%Cu/GDC10 was found the lowest coke deposition.

4.6 Acknowledgments

The author is grateful for the partial scholarship and partial funding of the thesis work provided by the National Excellence Center for Petroleum,

Petrochemicals, and Advanced Materials. The author also would like to acknowledge Asst. Prof. Siriporn Jongpatiwut for TPR and TPO study.

4.7 References

[1] Huang, G., Liaw, B., Jhang, C., and Chen, Y. (2009) Steam reforming of methanol over CuO/ZnO/CeO_2/ZrO2/Al_2O_3 catalysts. Applied Catalysis A: General, 358, 7-12.

[2] Liu, Y., Hayakawa, T., Suzuki, K., Hamakawa, S., Tsunoda, T., Ishii, T., and Kumagi, M. (2002) Highly active copper/ceria catalysts for steam reforming of methanol. Applied Catalysis A: General, 223, 137-145.

[3] Palo, D.R., Dagle, R.A., and Holladay, J.D. (2007) Methanol steam reforming for hydrogen production. Chemical Reviews, 107, 3992-4021.

[4] Kikuchi, E., Kawabe, S., and Matsukata, M. (2003) Steam reforming of methanol on Ni/Al_2O_3 catalyst in a Pd-membrane Reactor. Journal of the Japan Petroleum Institute, 46(2), 93-98.

[5] Dokmaingam, P., Laosiripojana, N., and Assabumrungrat, S. (2005, October) Hydrogen production from the methanol steam reforming over Ni/CeO2. The 15th Thailand Chemical Engineering and Applied Chemistry Conference, Jomtiem plam beach hotel and resort, Thailand.

[6] Jadhav, L.D., Chourashiya, M.G., Subhedar, K.M., Tyagi, A.K., and Patil, J.Y. (2009) Synthesis of nanocrystalline Gd doped ceria by combustion technique. Journal of Alloys and Compounds, 470, 383-386.

[7] Ksapabutr, B., Gulari, E., and Wongkasemjit, S. (2004). One-pot synthesis and characterization of novel sodium tris(glycozirconate) and cerium glycolate precursors and their pyrolysis. Materials Chemistry and Physics, 83, 34-42.

[8] Papavasiliou, J., Avgouropoulos, G., and Ioannides, T. (2007) Effect of dopants on the performance of CuO–CeO2 catalysts in methanol steam reforming. Applied Catalysis B: Environmental, 69, 226-234.

[9] Singh, A., and Hogarth, C.A. (1988) An infrared spectroscopic study of vacuum-evaporated SiO–CeO2 thin films. Journal of Materials Science, 23, 1090-1097.

[10] Brinker. C.J., and Scherer, G.W. (1990) Sol-Gel Science: The Physics and Chemistry of Sol-Gel Processing. San Diego: Academic Press.

[11] Phonthammachai, N., Rumruangwong, M., Gulari, E., and Jamieson., A.M., Jitkarnka, S., and Wongkasemjit, S. (2004). Synthesis and rheological properties of mesoporous nanocrystalline CeO_2 via sol–gel process. Colloids and Surfaces A: Physicochem. Eng. Aspects, 247, 61-68.

[12] Ksapabutr, B., Gulari, E., and Wongkasemjit, S. (2006). Sol-gel derived porous ceria powders using cerium glycolate complex as precursor. Materials Chemistry and Physics, 99, 318-324.

[13] Tanaka, K., and Ozaki, A. (1967) Acidity and catalytic activity of metal ions. Bulletin of the Chemical Society of Japan, 40, 1728-1730.

[14] Chalermnontakarn, A., and Wongkasemjit, S. (2007) Synthesis and property study of Ni-Cu/GDC 10 prepared via sol gel route to be used as ITSOFC anodes. Thesis, in The Petroleum and Petrochemical College, Chulalongkorn University, Bangkok.

[15] Tao, Y., Shao, J., Wang, J., and Wang, W.G. (2009) Morphology control of $Ce_{0.9}Gd_{0.1}O_{1.95}$ nanopowder synthesized by sol-gel method using PVP as a surfactant. Journal of Alloys and Compounds, 484, 729-733.

[16] Dan, L., Zhongyang, L., Chunjiang, Y., and Kefa, Cen. (2007) Study on agglomeration and densification behaviors of gadolinium-doped ceria ceramics. Journal of rare earths, 25, 163-167.

[17] Gurbani, A., Ayastuy, J.L., Gonzalez-Marcos, M.P., Herrero, J.E., Guil, J.M., and Gutierrez-Ortiz, M.A. (2009) Comparative study of CuO-Ceo2 catalysts prepared by wet impregnation and deposition-precipitation. International Journal of Hydrogen Energy, 34, 547-553.

[18] Wang, Y., Zhu, A., Zhang, Y., Au, C.T., Yang, X., and Shi, C. (2008) Catalytic reduction of NO by CO over NiO/CeO2 catalyst stoichiometric NO/CO and NO/CO/O2 reaction. Applied Catalysis B: Environmental, 81, 141-149.

[19] Fuentes, R.O., and Baker, R.T. (2009) Structural, morphological and electrical properties of $Gd_{0.1}Ce_{0.9}O_{1.95}$ prepared by a citrate complexation method. Journal of Power Sources, 186, 268-277.

[20] Huang, T., and Kung, Y. (2003) Effect of support modification on reduction and CO oxidation activity of doped ceria-supported copper oxide catalyst. Catalysis Letters, 85(1-2), 49-55.

[21] Trovarelli, A. (Eds.). (2002) Catalysis by ceria and related materials. London: Imperial College Press.

[22] Avgouropoulos, G., and Ioannides, T. (2003) Selective CO oxidation over $CuO\text{-}CeO_2$ catalysts prepared via the urea–nitrate combustion method. Applied Catalysis A: General, 244, 155-167.

[23] Pengpanich, S., Meeyoo, V., and Rirksomboon, T. (2004) Methane partial oxidation over $Ni/CeO_2\text{–}ZrO_2$ mixed oxide solid solution catalysts. Catalysis Today, 93-95, 95-205.

[24] Ocampo, F., Louis, B., and Roger, A. (2009) Methanation of carbon dioxide over nickel-based $Ce_{0.72}Zr_{0.28}O_2$ mixed oxide catalysts prepared by sol-gel method. Applied Catalysis A: General.

[25] Agrell, J., Lindstrom, B., Pettersson, L.J., and Jaras, S.G. (2002) Catalytic hydrogen generation from methanol. Catalysis, 16, 67-127.

[26] Oguchi, H., Nishiguchi, T., Matsumoto, T., Kanai, H., Utani, K., Matusumura, Y., and Imamura, S. (2005) Steam reforming of methanol over $Cu/CeO_2/ZrO_2$ catalysts. Applied Catalysis A: General, 281, 69-73.

[27] Ranganathan, E.S., Bej, S.K., and Thompson, L.T. (2005) Methanol steam reforming over Pd/ZnO and Pd/CeO_2 catalysts. Applied Catalysis A: General, 289, 153-162.

[28] Yasenava, P., Pavlova, S., Sadykov, V., Moroz, E., Burgina, E., Dovlitova, E., Rogov, V., Badmaev, S., Belochapkin, S., and Ross, J. (2008) Hydrogen production by steam reforming of methanol over Cu–CeZrYOx-based catalysts. Catalysis Today, 138, 175–182.

[29] Twigg, M.V., and Spencer, M.S. (2003) Deactivation of copper metal catalysts for methanol decomposition, methanol steam reforming and methanol synthesis. Topics in Catalysis, 22, 191-203.

[30] Li, Y., Guo, Y., and X, B. (2009) Catalytic combustion of methane over M (Ni, Co, Cu) supported on ceria-magnesia. Fuel Processing Technology, 90, 652-656.

[31] Biswas, P., and Kunzru, D. (2007) Steam reforming of ethanol for production of hydrogen over Ni/CeO_2–ZrO_2 catalyst: Effect of support and metal loading. International Journal of Hydrogen Energy, 32, 969-980.

[32] Laosiripojana, N., and Assabumrungrat, S. (2007) Catalytic steam reforming of methane, methanol, and ethanol over Ni/YSZ: The possible use of these fuels in internal reforming SOFC. Journal of Power Sources, 163, 943–951.

[33] Qi, C., Amphlett, J.C., and Peppley, B.A. (2005) Methanol steam reforming over NiAl and Ni (M) Al layered double hydroxides (M=Au, Rh, Ir) derived catalysts. Catalysis Letters, 104, 57-62.

[34] Patel, S., and Pant, K.K. (2006) Activity and stability enhancement of copper–alumina catalysts using cerium and zinc promoters for the selective production of hydrogen via steam reforming of methanol. Journal of Power Sources, 159, 139–143.

[35] Papavasiliou, J., Avgouropoulos, G., and Ioannides, T. (2004) Production of hydrogen via combined steam reforming of methanol over CuO–CeO_2 catalysts. Catalysis Communications, 5, 231-235.

[36] Wilson, M.S. (2009) Methanol decomposition fuel processor for portable power applications. International Journal of Hydrogen Energy, 34, 2955-2964.